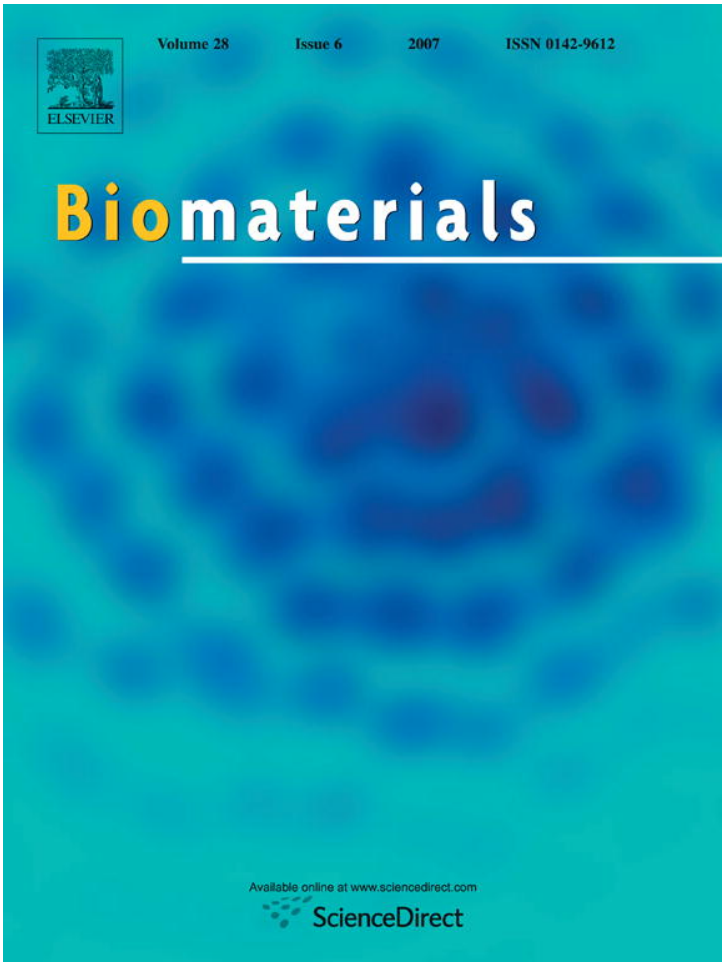

Available online at www.sciencedirect.com
ScienceDirect
Biomaterials 28 (2007) 916–926
Biomaterials
www.elsevier.com/locate/biomaterials

Coupled substitution of type A and B carbonate in sodium-bearing apatite

Michael E. Fleet*, Xi Liu

Department of Earth Sciences, University of Western Ontario, London, Ont., Canada N6A 5B7

Received 28 July 2006; accepted 4 November 2006

Abstract

A suite of Na-bearing type A–B carbonate hydroxyapatites $\{Ca_{10-y}Na_y[(PO_4)_{6-y}(CO_3)_y][(OH)_{2-2x}(CO_3)_x], x \approx y\}$ has been synthesized at 1200 °C and 0.5–1.0 GPa, and investigated by single-crystal X-ray structure and FTIR spectroscopy. Crystal data for the maximum content of carbonate (11.1 wt%) are $a = 9.3855(7)$, $c = 6.9142(4)$ Å, space group $P6_3/m$, $R = 0.023$, $R_w = 0.014$. Structural accommodation of the substitutions requires local coupling of Na and channel (type A) and phosphate (type B) carbonate ion defects. The type B carbonate ion is located on the sloping faces of the substituted phosphate group, but is inclined at an angle of 53° to the mirror plane. FTIR spectra have minimal v_3 absorption beyond 1500 cm^{-1} and dominant v_2 absorption at 873 cm^{-1}. Synthetic Na-bearing type A–B apatites (with a high content of type A carbonate) are thus similar in both chemical composition and infrared spectra to biological apatites. The latter are reinterpreted as Na-bearing type A–B carbonate apatites with channel carbonate up to 50% of total carbonate.

Keywords: Apatite structure; Hydroxyapatite; Biomineralisation; Bone; Crystallography

1. Introduction

Minor amounts of sodium and carbonate are important, and possibly essential, constituents of the hydroxyapatite of human dental enamel and bone (e.g. [1–8]). The average structure of end-member hydroxyapatite $[Ca_{10}(PO_4)_6(OH)_2]$ is well known (Fig. 1). It appears that the carbonate ion can substitute for both OH in the *c*-axis channel of apatite (type A carbonate) and the phosphate group (type B carbonate). These structural roles have been studied extensively by X-ray and neutron diffraction, chemical analyses, infrared (IR) and Raman spectroscopy, proton and ^{13}C NMR spectroscopy, and computer modeling [7–34]. Diffraction studies on the detailed structure of biological apatite have been limited by its very small crystal size, and most of our present understanding is inferred from studies on synthetic material, with much emphasis being placed on vibrational spectroscopy, particularly FTIR. It is presently understood that type A carbonate is characterized by a doublet band at about 1545 and 1450 cm^{-1} (asymmetric stretch vibration, v_3) and a singlet band at about 878 cm^{-1} (out-of-plane bend vibration, v_2), whereas type B carbonate has these bands at about 1455, 1410 and 873 cm^{-1}, respectively.

Recent single-crystal X-ray and FTIR studies on types A and A–B carbonate apatites synthesized at high temperature and pressure, with an overall composition of $Ca_{10}(PO_4)_{6-y}(CO_3)_{x+(3/2)y}(OH)_{2-2x}$ ($y = 0$–0.82; $x = 0.5$–0.75), determined the orientation and environment of the A and B carbonate ions [30–33]. The results for the channel carbonate ion in a type A carbonate apatite were in good agreement with defect structures calculated using static lattice DFT [21] and energy minimization/molecular dynamics [34] methods. However, the crystal chemical information on type B carbonate in A–B carbonate apatites was tentative because only one of the carbonate oxygens was identified, with the other two considered to be hidden by overlap with O1 and O2. Also, the angle of

*Corresponding author. Tel.: +1 519 661 3184; fax: +1 519 661 3198.
E-mail addresses: mfleet@uwo.ca (M.E. Fleet), xliu258@uwo.ca (X. Liu).

0142-9612/$ - see front matter © 2006 Elsevier Ltd. All rights reserved.
doi:10.1016/j.biomaterials.2006.11.003

inclination to the basal plane (0 0 1) (50–60°) was appreciably greater than that inferred from polarized IR study of francolite (37 °C) [11] and neutron powder diffraction study of a synthetic Na-bearing type B carbonate apatite (~30°) [8]. We presently continue study of this discrepancy, investigating a suite of Na-bearing type A–B carbonate apatites synthesized at high temperature and moderate pressure.

2. Experimental

High-pressure experiments to synthesize sodium- and type B-carbonate-substituted hydroxyapatite were made using a Depths of the Earth Company Quickpress piston-cylinder device and a $\frac{3}{4}$ inch assembly. Starting compositions were prepared from analytical grade $CaHPO_4$, Na_2CO_3, $Ca(OH)_2$, and $CaCO_3$. These salts were mixed in stoichiometric proportions corresponding to an ideal carbonate apatite formula of $Ca_{10-y}Na_y[(PO_4)_{6-y}(CO_3)_y](OH)_2$ with $y = 2$ or 3 and excess fluid (Table 1); e.g. $4CaHPO_4 + Na_2CO_3 + 2Ca(OH)_2 + 2CaCO_3$ corresponds to $Ca_8Na_2[(PO_4)_4(CO_3)_2](OH)_2 + 3H_2O + CO_2$. While $CaHPO_4$ was used without any drying, Na_2CO_3, $Ca(OH)_2$ and $CaCO_3$ were dried at 200 °C and 1 atm for 48 h, and the starting mixtures were mixed and ground under acetone in an agate mortar. For each experiment, the starting mixture was encapsulated in a sealed platinum tube with a diameter of 5 mm and a height of 10 mm. The capsule was separated from a graphite tube by an MgO sleeve. Run conditions for the four experiments reported in this study are given in Table 1. All experiments were quenched at pressure by switching off the furnace.

The products were characterized by optical microscopy, powder X-ray diffraction (Rigaku D/MAX-B system; Co Kα X-radiation), electron probe micro-analysis (JEOL JXA-8600, using a lead stearate spectrometer crystal for carbon; Table 2), and FTIR spectroscopy (Nicolet Nexus 670 FTIR spectrometer). The IR spectra were obtained for hand-separated carbonate apatite crystals using KBr pellets (Fig. 2). About 10 mg of apatite crystal product was first ground to a powder, then diluted in an agate mortar with 1 g of KBr and ground under an IR heating lamp to a grain size <25 μm. Transparent pellets were made under vacuum at a pressure of 200 kg/cm^2.

Single-crystal fragments from experiments LM005 and LM006 (Tables 1 and 2) were prepared by trimming prismatic grains of carbonate apatite with a scalpel blade and evaluated for X-ray structure analysis by optical microscopy. Single-crystal measurements were made at room temperature and pressure with a Nonius Kappa CCD diffractometer and graphite-monochromatized Mo Kα X-radiation (50 kV, 32 mA, $\lambda = 0.7107$ Å). Procedures for data reduction and structure analysis followed our previous studies [30–33]. Relevant experimental details are given in Table 3, and final parameters for LM005 in Table 4. Lists of structure factors are available from the first author.

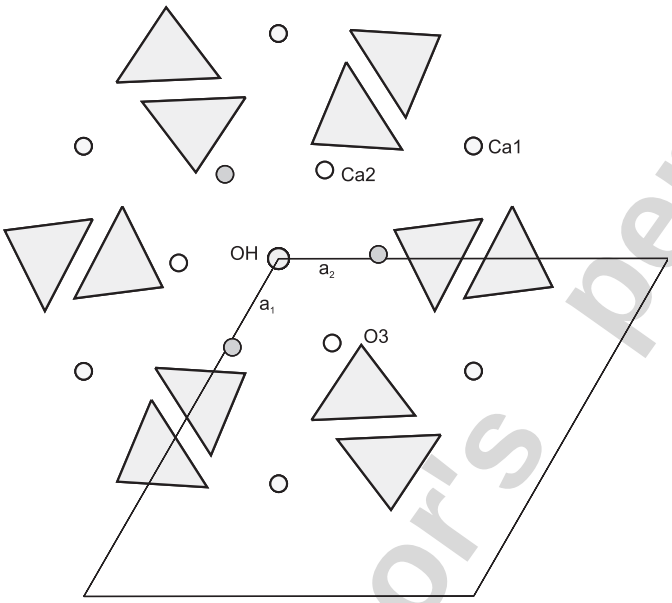

Fig. 1. Structure of hydroxyapatite [$Ca_{10}(PO_4)_6(OH)_2$] viewed along *c*-axis: PO_4 tetrahedra (triangles) are interconnected by large cations (Ca1, Ca2), and Ca2 cations and O3 oxygens form inner wall of apatite channel.

3. Results

3.1. Experimental products

The products of the synthesis experiments consisted of prismatic apatite crystals (up to 800 μm in length) and fine-grained matrix material. The latter consisted of apatite and minor-trace carbonate in LM002 and LM003, with rather more carbonate in LM006. In contrast, LM005 yielded only anhydrous products, indicating that the capsule had lost H_2O (or H_2) during the course of the experiment. However, the apatite crystals from LM005 formed thicker prisms (up to $50 \times 50 \times 500$ μm^3) and were of better diffraction quality than in the other experiments, and contained the highest carbonate content (Table 2; Fig. 2).

3.2. FTIR spectroscopy

The FTIR spectra reveal significant amounts of structural carbonate in all four synthetic apatites (Fig. 2). The areas of the v_3 and v_2 bands increase progressively with

Table 1
Piston cylinder experiments for synthesis of carbonate apatite

Expt	*T* (°C)	*P* (GPa)	Time (h)	Starting composition		
				y[a] (pfu)	Fluid H_2O (mol pfu)	CO_2 (mol pfu)
LM002	1200	1.0	8	2	3	1
LM003	1200	1.0	8	2	1	3
LM005	1200	0.5	8	2	3	1
LM006	1200	1.0	16	3	0.5	2.5

[a]Ideal formula: $Ca_{10-y}Na_y[(PO_4)_{6-y}(CO_3)_y](OH)_2$.

Table 2
Composition of synthetic Na-carbonate-bearing apatites[a]

Experiment/oxide	LM002	LM003	LM005	LM006
P_2O_5	41.2(3)	39.7(8)	36.7(3)	40.3(4)
CaO	55.7(3)	54.6(4)	52.4(5)	55.2(8)
Na_2O	0.34(8)	1.16(12)	2.76(11)	1.09(13)
CO_2	2.8(4)	4.6(8)	8.2(2)	3.5(7)
Total	100.0	100.1	100.1	100.1
Formula amounts[b]				
Ca	9.89	9.63	9.13	9.66
Na	0.11	0.37	0.87	0.35
P	5.77	5.54	5.05	5.56
C (B type)	0.23	0.46	0.95	0.44
C (A type)	0.41	0.56	0.86	0.33

[a]Electron microprobe analysis.
[b]Relative to ideal formula [Table 1, footnote (a)].

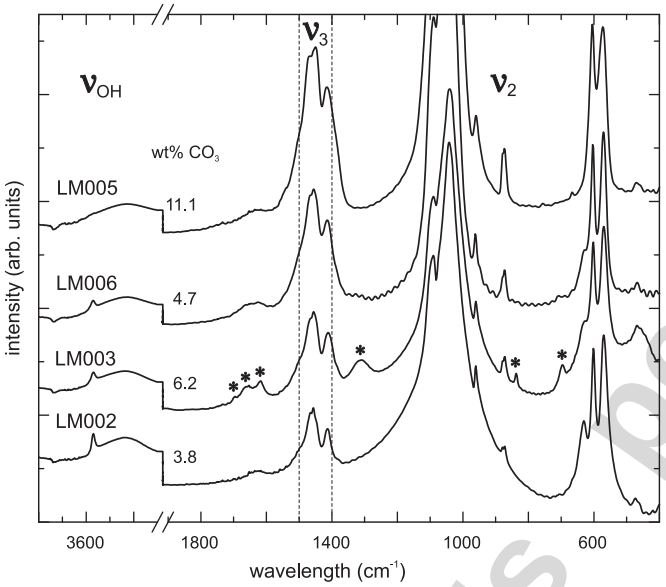

Fig. 2. FTIR spectra for suite of Na-bearing type A–B carbonate apatites, identifying bands due to OH stretching (ν_{OH}) and asymmetric stretching (ν_3) and out-of-plane bending (ν_2) of carbonate ions, as well as bands attributable to bicarbonate ion in LM003 (*): note that strength of carbonate bands increases with increase in total carbonate content determined by electron microprobe.

increase in the analyzed amounts of total carbonate for LM002, LM006 and LM005, which are 3.8, 4.7 and 11.1 wt%, respectively. Relative to the height of the phosphate asymmetric bend mode band (at 573 and 605 cm^{-1}), LM005 has a similar amount of carbonate to a Na-free carbonate apatite with 11.13 wt% carbonate [23] and slightly less carbonate than a (Ca, Na) carbonate apatite with 12.50 wt% carbonate [8]. The ν_3 and ν_2 bands are composite and have similar forms in all four apatites. The ν_3 absorption intensity is broadly confined within the interval 1400–1500 cm^{-1} and, for LM005, is represented by peaks at 1416, 1449 and 1473 cm^{-1}. Peak positions and band areas obtained from spectra fitted with Gaussians using program BGAUSS [35; 30,31; Fig. 3] are summarized in Table 5. Evidently, there are numerous discrete carbonate environments in these apatites, and the ν_3 region cannot be readily deconvoluted into overlapped symmetrical doublets. The ν_2 region is also composite with a dominant peak at 873 cm^{-1}, and a shoulder at 880 cm^{-1} representing only 10–15% of the total band intensity. The OH stretch band (at 3570 cm^{-1}) and OH libration band (at 631 cm^{-1}) both decrease in intensity progressively with increase in carbonate content (Fig. 2), and there is no evidence of structurally bound OH in LM005. An added complication for apatite LM003 is the appearance of bands (marked by an asterisk in Fig. 2) that are attributable to the bicarbonate ion (HCO_3^-) and probably represent admixed sodium bicarbonate.

3.3. X-ray structure refinements

The electron microprobe analyses revealed that we had, in fact, synthesized a suite of Na-bearing type A–B carbonate apatites (Table 2) rather than the type B carbonate hydroxyapatites of ideal formula $Ca_{10-y}Na_y[(PO_4)_{6-y}(CO_3)_y](OH)_2$ anticipated at the outset of this study. Moreover, Na and types A and B carbonate are present in approximately equal amounts, consistent with a substitution formula of the type $Ca_{10-y}Na_y[(PO_4)_{6-y}(CO_3)_y][(OH)_{2-2x}(CO_3)_x]$, with $x \approx y$. Single-crystal X-ray structure analyses were made on apatite from experiments LM005 and LM006. The stoichiometric coefficient y was close to unity for the apatite product of LM005, and in the range 0.35–0.45 for LM006.

X-ray structure refinement of LM005 in the hexagonal space group $P6_3/m$ generally followed the previous studies on type A–B carbonate apatites [31–33], except that the scattering factors and dispersion corrections for the Ca1 and Ca2 positions were weighted in proportion to the formula amounts of Ca and Na given in Table 2. The structure refinement confirmed that Ca1 and Ca2 were essentially fully occupied by (Ca + Na). On the other hand,

Table 3
Experimental details for X-ray structures

Experiment	LM005	LM006
Crystal	xt391	xt390
Crystal size ($mm^3 \times 10^3$)	0.14	0.22
Crystal shape	Prism	Prism
a (Å)	9.3855(7)	9.3965(13)
c (Å)	6.9142(4)	6.8894(14)
Formula weight	990.5	998.4
D_x (g/cm^3)	3.12	3.15
Reflections—unique	562	557
Number, with ($I<3\sigma_{(I)}$)	416	281
R_{Int}	0.057	0.046
Refined parameters	40	41
R	0.023	0.027
R_w	0.014	0.023
S	0.60	1.48
Extinction ($\times 10^4$)	1.63(6)	0.95(6)
$\Delta\rho$ ($eÅ^{-3}$) (+)	0.26	0.74
(−)	0.36	0.47

Table 4
Synthetic A–B carbonate apatite[a]: positional and isotropic thermal parameters for LM005

	Equipoint; site occupancy	x	y	z	U,U_{eq}
Ca1	4*f*; 0.969(3)	2/3	1/3	0.0014(1)	0.0193(6)
Ca2	6*h*; 0.987(2)	0.9875(1)	0.2499(1)	1/4	0.0181(4)
P	6*h*; 0.871(7)	0.3691(2)	0.3977(2)	1/4	0.0145(7)
O1	6*h*; 0.871(7)	0.4780(3)	0.3232(3)	1/4	0.0151(9)
O2	6*h*; 1.0	0.4644(3)	0.5816(3)	1/4	0.0341(9)
O3	12*i*; 0.903(8)	0.2556(3)	0.3395(3)	0.4263(3)	0.041(1)
C1	12*i*; 0.083[b]	0.046(1)[c]	0.065(1)	0.492(1)	0.025[d]
O5	12*i*; 0.083	0.144(1)	0.220(1)	0.472(1)	0.025
O6	12*i*; 0.083	0.005(1)	0.002(1)	0.662(1)	0.025
O7	12*i*; 0.083	−0.010(1)	−0.028(1)	0.343(1)	0.025
O8	12*i*; 0.064(4)	0.345(3)	0.424(3)	0.448(3)	0.025
O9	6*h*; 0.129(8)	0.512(2)	0.361(2)	1/4	0.025

[$Å^2$; $U_{eq} = (1/3)\ \Sigma_i\Sigma_j\ U^{ij}\ a^i a^j\ a_i.\ a_j$].
[a]Space group $P6_3/m$.
[b]Occupancies of C1–O7 correspond to one type A carbonate ion pfu.
[c]x, y, z for C1–O7 from rigid body refinement.
[d]U of C1–O9 not refined.

the occupancies of P and O3 were significantly less than unity (equivalent to 5.23 and 10.84 atoms of P and O3 per unit cell), and consistent with substitution of the phosphate group by the carbonate ion.

Residual electron density within the apatite channel was readily associated with atoms of type A carbonate (i.e. the positions C1, O5, O6, and O7; Table 4). Open refinement of the channel carbonate atoms of LM005 resulted in occupancies of 0.092(3) for C1, 0.073(3) for O5, and 0.176(10) for overlapped O6/O7; thus indicating that the channel carbonate (type A) positions were essentially fully occupied. We have emphasized in earlier X-ray structure studies on type A–B carbonate apatite [31–33] that, for space group $P6_3/m$, the electron densities for atoms of the A and B carbonate ions are each distributed over 12 equivalent positions with partial occupancy, and the maximum occupancy for channel carbonate atoms in the disordered structure is 1/12 (or 0.083). The refined occupancy of the channel hydroxyl oxygen (O4) was −0.01(1), confirming the conclusion from the FTIR study that LM005 did not contain structural water. Therefore, O4 is not reported in Table 4. Also, there was no evidence of type A2 carbonate, which occupies a stuffed channel position in Na-free type A–B apatites synthesized at somewhat higher pressure [31–33]. In summary, the X-ray structure of LM005 showed that the apatite channel was singly occupied by one type A carbonate per unit cell. In the final structure, C1, O5, O6, and O7 were located by rigid body refinement of the type A carbonate ion, following the procedure of Fleet and Liu [33], and using atom occupancies of 0.083 and fixed isotropic displacement parameters (U) of 0.025 $Å^2$ (Table 4).

There was also weak residual electron density in the general vicinity of O3 and close to O1, which was assigned to two oxygen atoms of the type B carbonate ion, labeled O8 and O9, respectively. O8 was reported for all five type A–B apatites investigated in earlier studies [31–33], where it was labeled OB3 and interpreted similarly as an oxygen atom of a type B carbonate ion located close the sloping faces of the PO_4 tetrahedron. The other two oxygen atoms of this putative type B carbonate ion were considered to be hidden by overlap with O1 and O2. The third carbonate oxygen in the present structure was located too close to O2 to be separately resolved from it. The electron densities of O8 and O9 were consistent with the loss in density of P and O1. Therefore, assuming that small discrepancies in occupancies represent systematic errors close to the limit of resolution, unit-cell contents were constrained according to: O1 = P; and O8 = O9 = (6 – P) (Table 4). It is well known (e.g. [11,22,36,37]) that the occupancy of the phosphorus position yields the most reliable estimate of the extent of substitution by type B carbonate. The positional coordinates of O8 and O9 were refined separately from the other variable parameters, because of the close proximity of O9–O1. There was also weak electron density at the position of the carbon atom (C2) but this was too diffuse for meaningful refinement. There was no significant electron density at other possible carbon positions on the sloping and vertical faces of the substituted PO_4 tetrahedron.

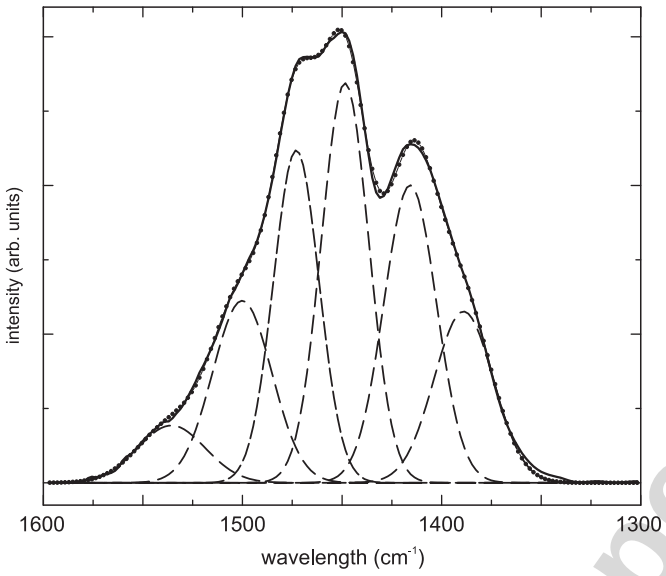

Fig. 3. Asymmetric stretch (ν_3) region of the FTIR spectrum for the Na-bearing carbonate apatite LM005 fitted with Gaussian distributions corresponding to the peaks and shoulders evident in envelope.

Preliminary refinement of the carbonate apatite from experiment LM006 showed that the stoichiometric coefficients x and y in the substitution formula were about 0.5 and 0.4, respectively. Thus, electron densities for the oxygen atoms of the type A carbonate were about one-third of that of a hydrogen atom. Therefore, the LM006 structure was refined similarly to that of LM005, except that the hydroxyl oxygen (O4) was included, resulting in 1.07(2) OH pfu, the positional parameters of the carbonate atoms C1 and O5–O9 were taken from LM005, and unit-cell contents were constrained as follows: O5 = O6 = O7 = C1; O8 = O9 = (6 – P); O1 = P; and O3 = [12 – (6 – P)]. We presently report only experimental details (Table 3) and formula amounts of carbonate (Table 6) for this X-ray structure.

4. Discussion

4.1. Composition of synthetic apatite

The synthesis experiments resulted in a suite of Na-bearing type A–B carbonate apatites (Table 2) of ideal formula

Table 5
Fitted FTIR spectra

Apatite	ν_3 bands				ν_2 bands	
	Principal		Subordinate			
	Position (cm^{-1})	Area[a]	Position (cm^{-1})	Area	Position (cm^{-1})	Area
LM002	1414	1.80	1386	0.23	872	0.24
	1453	2.59	1501	1.11	880	0.04
	1472	1.87	1532	0.32		
LM003	1412	2.90	1390	0.48	872	0.45
	1452	3.54	1502	1.46	880	0.05
	1474	2.49	1532	0.41		
LM006	1415	4.53	1389	1.36	873	0.68
	1450	5.21	1501	2.69	880	0.07
	1473	4.36	1532	0.95		
LM005	1416	6.61	1389	4.29	873	1.30
	1449	8.02	1500	4.57	880	0.17
	1473	6.43	1536	1.64		

[a]Arbitrary units.

$Ca_{10-y}Na_y[(PO_4)_{6-y}(CO_3)_y][(OH)_{2-2x}(CO_3)_x]$ (Tables 2, 6 and 7), with $x \approx y$. The formula amounts estimated by three independent methods (electron microprobe, X-ray structure refinement, and FTIR band area) are reasonably consistent (Table 6), taking into account that the FTIR band areas for LM003 represent only part of the total carbonate content. LM005 contains the highest carbonate content. Based on the X-ray structure analysis, this apatite has the full complement of channel (type A) carbonate ions and is anhydrous, with the approximate formula $Ca_9Na[(PO_4)5(CO_3)](CO_3)$. Our experimental method did not yield type B carbonate hydroxyapatite $[Ca_{10-y}Na_y[(PO_4)_{6-y}(CO_3)_y](OH)_2]$ as intended, due to the high partial pressure of CO_2 [$p(CO_2]$ and the preferential partitioning of sodium into the melt/fluid phase. On the other hand, LM005 apatite proved to be crucial for understanding the incorporation of carbonate in type A–B apatite, and we believe that the structure of LM006 is a good approximation to the structure of carbonated hydroxyapatite in bone and enamel (Table 7).

4.2. Location of carbonate ions

The type A carbonate ion in the apatite channel of LM005 is located similarly to the type A1 carbonate ions in the A–B apatite structures of our previous studies [31–33]. Relative to the model channel structure with the carbon atom on the *c*-axis (Fig. 4), the type A carbonate ion is rotated clockwise by 9° and canted $<1°$, compared with a similar rotation and a canting angle of 7° for the type A1 carbonate of the type A–B carbonate apatite PC55 [31] and a counterclockwise rotation of $\sim 11°$ and canting angle of 9° for channel carbonate in the type A carbonate apatite PC71 [30,33]. These observed orientations in synthetic apatites are similar to those for channel carbonate ions in defect structures calculated using static lattice DFT [21] and energy minimization/molecular dynamics [34] methods, except that the axial oxygens (O6, O7 in this study) are more-or-less symmetrically positioned with respect to $z = 0.0$ and 0.5 in our studies. The lack of significant canting and the symmetrical positioning of the carbonate

Table 6
Estimates of formula amounts of types A and B and total (A + B) carbonate

Experiment	Microprobe analysis			X-ray structure			FTIR band area[a]	
	A	B	Total	A	B	Total	ν_3	ν_2
LM002	0.41	0.23	0.64	—	—	—	0.44	0.34
LM003	0.56	0.46	1.02	—	—	—	0.63	0.58
LM005	0.86	0.95	1.81	1.0	0.77	1.77	1.77	1.77
LM006	0.33	0.44	0.77	0.52	0.38	0.90	1.07	1.02

[a]Normalized to 1.77 for LM005.

Table 7
Compositions of synthetic carbonate apatites and bovine bone (wt%)[a]

	LM005	RMW04	Mon 8	LM006	Bovine bone	Enamel	
Ca	37.4	35.4	37.2	39.5	36.6	37.6	
P	16.0	18.5	20.3	17.6	17.1	18.3	
CO_2	8.2	9.2	8.2	3.5	4.8	3.0	
Na	2.05	2.89	—	0.81	1.0	0.7	
K	—	—	—	—	0.07	0.05	
Mg	—	0.13	—	—	0.6	0.2	
Al	—	0.04	—	—	—	—	
Sr	—	0.02	—	—	0.05	0.03	
Ba	—	0.01	—	—	—	—	
Cl	—	—	—	—	0.1	0.4	
F	—	—	—	—	0.1	0.01	
Formula amounts							
	Ca	Na	PO_4	CO_3	OH	CO_3	H_2O
LM005	9.13	0.87	5.05	0.95	—	0.86	—
LM005-ideal	9	1	5	1	—	1	—
RMW04	8.09	1.27	4.09	1.91	1.36	—	1.91
Mon 8	8.24	—	4.34	1.66	0.14	—	2.29
LM006	9.66	0.35	5.56	0.44	1.34	0.33	—

[a]References: RMW04 [8]; Mon 8 [23]; bovine bone and enamel [5], representing 73 wt% of dry fat-free bone and ash content, respectively.

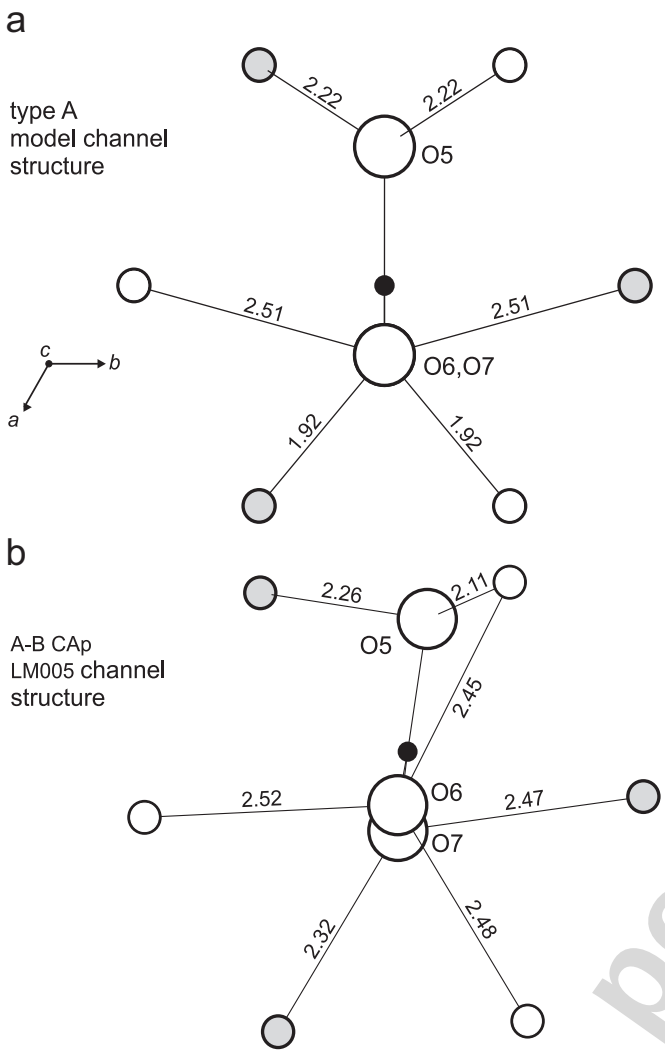

Fig. 4. Orientation of type A carbonate ion in apatite channel, viewed along *c*-axis: Ca2 cations are in channel wall at unit-cell heights of $z \approx 0.25$ (shaded circles) and $z \approx 0.75$ (open circles), and carbon atom is at $z \approx 0.5$: (a) model structure with Ca2 at 0.25 and 0.75 and carbon at 0.5; (b) Na-bearing type A–B carbonate apatite (CAp; LM005); bond distances are Å.

ion in the apatite channel reflects the absence of other channel constituents in apatite LM005: the occupancy of the type A carbonate in this carbonate apatite is essentially 1.0. In comparison, carbonate ions were in competition with hydroxyl ions (and possible H_2O, as well) in the *c*-axis channels of the previously studied types A [30] and A–B apatites [31,32]. The channel carbonate of LM005 has a more equitable distribution of bond distances to Ca2 cations than the previous A–B apatite structures, and O6 forms a relatively short bond of 2.45 Å to the third Ca2 cation at $z = 0.75$. This O6–Ca2 distance compares with 2.68 Å in PC55 and 2.98 Å in the model structure of Fig. 4a. It is a bonded distance in LM005 because the A carbonate ion is displaced to one side of the apatite channel, with O6 and O7 almost coincident with the *c*-axis and O5 extending 2.39 Å outwards close to the channel wall and very close to an O3 atom of the phosphate group in the average structure (Fig. 5a). The O5–O3 distances are 1.14, 2.43 and 2.80 Å in LM005, and 1.30, 2.61 and 2.75 Å in PC55 [31]. The short O5–O3 distance in the average structure of LM005 is relaxed local to B carbonate ions in the real A–B carbonate apatite structure (see below) by either local omission of O3 or local displacement of O3–O8. In comparison, in type A carbonate apatite the carbonate ion is centrally located in a dilated apatite channel [30], resulting in O5–O3 distances of 2.07 and 2.24 Å. These differences in local accommodation readily account for the opposite rotations and different canting angles of the channel carbonate ion in types A and A–B carbonate apatite.

The interatomic oxygen–oxygen distances for the type B carbonate ion in LM005 (O8–O9 = 2.38, O9–O2 = 2.33, and O2–O8 = 1.92 Å) are known only approximately due to systematic errors in refining the oxygen atom positions from weak and overlapped electron density, and do not represent anomalous distortion of the carbonate ion geometry. The electron density of the type B carbon atom (C2) was too weak and diffuse for meaningful refinement, and has not been included in Table 4 and Fig. 5.

The close approach (1.14 Å) in the average structure of O5 to an O3 atom of the phosphate group suggests that the A and B carbonate ions have to be coupled in the A–B apatite structure, so that the bulky channel carbonate ion uses some of the space created in the type B carbonate-for-phosphate substitution. Clearly, O3 cannot be occupied locally, or must be pushed away to O8, to accommodate the off-axis oxygen (O5) of the channel carbonate ion (Fig. 5). Coupling is also suggested by similarity of the formula contents of Na and types A and B carbonate, particularly for LM005 and LM006 (Tables 2 and 6). Thus, although the substitution mechanisms for the types A and B carbonate ions are generally considered separately, they appear to be coupled by a structural constraint in the present A–B carbonate apatites.

There remains some ambiguity in the precise orientation of the type B carbonate ion in the A–B carbonate apatite structure. Fig. 5 illustrates alternative ways of pairing types A and B carbonate ion defects in hydroxyapatite. In Fig. 5a, the O3 atom closest to O5 is displaced to O8. However, the O5–O8 distance of 2.01 Å is still short, and there seems no need on space-filling grounds alone to remove the other O3 atom (O3′) of the substituted phosphate group from the structure. In Fig. 5b, O3′ is displaced to O8′, and O3 is removed from the structure, consistent with the substitution scheme:

$$[Na + {}^{B}CO_3 = Ca + PO_4].$$

Logically, Na in the Ca2 position is used for local charge balancing in both cases, and should be the nearest large cation to the O3 vacancy. We recognize that the refined occupancy of the O3 position (Table 4) suggests that only 0.39 atoms pfu of O3 have been removed from the structure (with 0.77 displaced to O8), but the occupancy

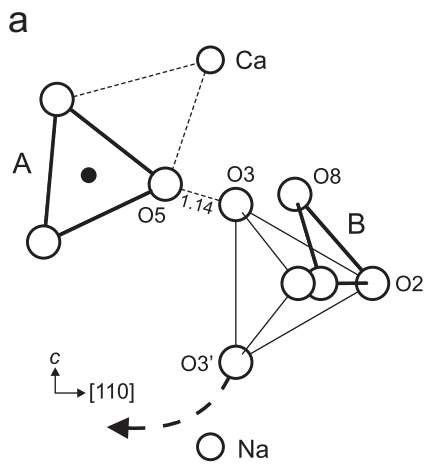

Fig. 5. Alternative ways of coupling a Na cation and A and B carbonate ion defects in hydroxyapatite. The A and B carbonate ions have to be paired because the off-axis oxygen (O5) of the type A carbonate is pushed too close to an O3 oxygen of the phosphate group in the average structure. In the local structure, O3 is either displaced to O8 as in part (a) or removed from the structure as in part (b), and the Na cation helps to charge balance the oxygen vacancy: bond distances are Å.

refinement of O3 is limited by the anomalously large anisotropic displacement for this position [32].

In LM005, the angle of inclination of the type B carbonate ion to the basal plane (0 0 1) is 53° and, thus, remains appreciably greater than that deduced for francolite (37°) [11] and Na-bearing carbonate apatite (~30°) [8]. This discrepancy may simply reflect differences in synthesis/crystal growth conditions and composition, since the channel position is blocked to the carbonate ion by fluoride in francolite and hydroxyl ions in the Na-bearing apatite, which was prepared by precipitation in near-boiling aqueous solution. When type A carbonate is either not present or a very minor component, it would seem unnecessary for O3 of a substituted phosphate group to be pushed away from the apatite channel. However, the second O3 atom (O3′) does have to be omitted or displaced to non-bonded distances with the B carbonate oxygen. Carbonate ion orientations parallel to the sloping faces of the substituted phosphate tetrahedron [8,11] and lying on the mirror plane at $z = 0.25, 0.75$ [27] are certainly possible for other (type B carbonate) apatites, but resolution of these structural details must await single-crystal X-ray structure study of francolite and synthetic type B carbonate apatites.

4.3. Interpretation of FTIR spectra

The absence of significant IR absorption intensity beyond 1500 cm^{-1} in the asymmetric stretch (ν_3) region and dominance of the 873 cm^{-1} band in the out-of-plane bend (ν_2) region are generally understood to be characteristic of type B carbonate apatite [5,23,28]. The ν_3 region for the present series of type A–B carbonate apatites increases in intensity progressively with increase in carbonate content, but maintains the same overall position and form (Fig. 2; Table 5). This behavior is consistent with maintenance of the coupling between Na and types A and B carbonate at all carbonate contents investigated. The single-crystal X–ray structure of apatite from experiment LM005 showed unambiguously that the apatite channel is fully occupied by type A carbonate, and there is a substantial but slightly lower content of type B carbonate substituting for the phosphate group. Thus, the ν_3 region of the FTIR spectrum of LM005 (Figs. 2 and 3) must represent intensity from type A carbonate as well as from type B carbonate. If the band assignments of Fleet et al. [32] are followed, the symmetrical doublet bands at 1416 and 1473 cm^{-1} in Fig. 3 are associated with the type B carbonate ion in a single structural environment. The remaining intensity, including the prominent band at 1449 cm^{-1}, must then be associated with the type A carbonate absorption and represents a composite of multiple carbonate stereochemical environments in the apatite channel. However, regardless of the individual band assignments, the important point from this section is that about 57% of the composite ν_3 region intensity, which is largely limited to the 1400–1500 cm^{-1} spectral interval, represents type A carbonate.

The types A and A–B carbonate apatites discussed in our previous studies [30–33] had appreciable ν_3 region absorption intensity at wavenumbers beyond 1500 cm^{-1} (Fig. 6): note that, for the type A–B apatite PC55, the ν_3 intensity beyond 1500 cm^{-1} is enhanced by absorption from carbonate in the stuffed channel position (A2), and the intensity of the 1406 cm^{-1} band is enhanced due to interference from admixed calcite. Both PC71 and PC55 in Fig. 6 are Na-free carbonate apatites with essentially a full complement of Ca in Ca1, Ca2 positions: PC71 was almost exclusively type A carbonate apatite, with substitution scheme:

$$[^{A}CO_3 = 2OH]$$

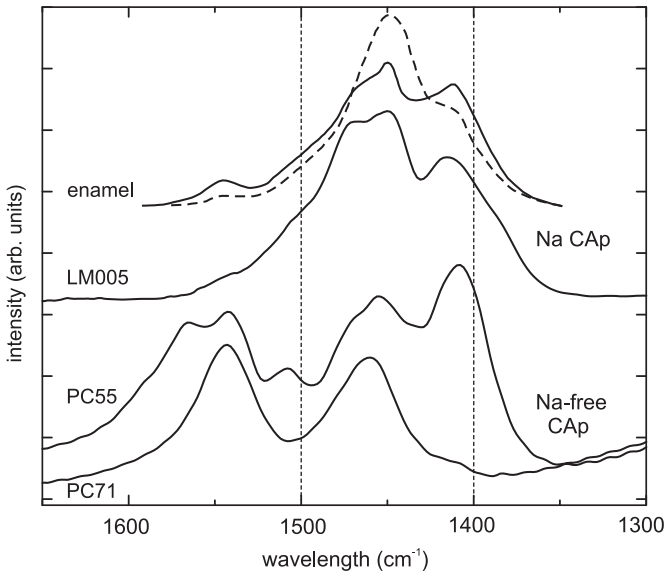

Fig. 6. Asymmetric stretch (v_3) region of the FTIR spectra for Na-free type A (PC71) [30] and type A–B (PC55) [31] carbonate apatites (CAp) and Na-bearing type A–B carbonate apatite (LM005) compared with corresponding polarized IR spectrum of human dental enamel [9]: note that v_3 absorption for type A carbonate in the two Na-free apatites extends beyond 1500 cm^{-1}.

and the type B carbonate-for-phosphate substitution in PC55 was more-or-less charge balanced by the entry of carbonate into the stuffed channel position:

$$[^{A2}CO_3 + 2^{B}CO_3 = {}^{A2}\square\sim + 2PO_4].$$

In contrast, LM005 is a Na-bearing type A–B carbonate apatite. The type B carbonate-for-phosphate substitution is now charge balanced by the entry of Na cations into Ca1, Ca2 positions, and the v_3 region absorption for the type A carbonate is displaced almost exclusively into the 1400–1500 cm^{-1} spectral interval (cf., Fig. 6). These limited results for carbonate apatite synthesized at moderate and high pressure suggest a significant control by the composition of Ca1, Ca2 sites on the position of the v_3 bands for type A carbonate. Indeed this correlation may be extended to numerous literature studies, including [14,19,25] for Na-free and [1,7,16,38] for Na-bearing type A–B carbonate apatites.

Although a dependence of v_3 band position on apatite composition (Na-free Versus Na-bearing) is presently established for the type A carbonate component, its crystal-chemical explanation is not readily apparent. The position and half width of the v_3 doublet bands for the type B carbonate component in hydroxyapatite appear to vary little with bulk composition and conditions of synthesis, and the centroid for these bands is close to the v_3 vibrational frequencies of the alkaline earth carbonates [39]. On this basis, the displacement of the centroid of type A carbonate in Na-free apatite to about 1500 cm^{-1} (e.g. Fig. 6) could be considered to be the anomalous feature. Moreover, the greater dispersion of the v_3 bands for type A carbonate ([31,32]; Fig. 3) suggests that type A is more sensitive to small changes in local stereochemical environment than type B carbonate. On the other hand, the creation of Ca1, Ca2 vacancies and local imbalance of charge through substitutions like:

$$[0.5^{Ca}\square\sim + CO_3 = 0.5Ca + PO_4]$$

do not appear to exert a significant effect on the position of v_3 region absorption for type A carbonate. Hydrogen bonding in the apatite channel is not a significant factor either for the present synthetic carbonate apatites. In principle, hydrogen bonding to carbonate oxygens would transfer bond valence away from the carbon–oxygen bonds, shifting the v_3 absorption for type A carbonate to lower wavenumbers. However, LM006, LM003 and LM002, with mixed occupancies of OH, CO_3 in channel positions, have the same v_3 region profile as LM005, an anhydrous carbonate apatite.

We have suggested above that the accommodation of type A carbonate in Na-bearing A–B carbonate apatites requires coupling between the formula contents of Na and types A and B carbonate. Also, the lack of correlation between the shift in position and profile of v_3 bands and content of Na (Fig. 2; Tables 2 and 5) confirms that the A and B carbonate ions, Na cations and O3 vacancies occur as clustered defects within the apatite structure, as illustrated in Fig. 5. The Na cation is more closely related to the A carbonate in Fig. 5b. The short Na–O5 bond (2.11 Å) and the bonded Na–O6 distance might draw O5 and O6 bond strength away from the carbon atom (C1) and, thus, contribute to displacement of the type A v_3 bands to lower wavenumbers. The relatively high dispersion of these bands is readily attributable to multiple local stereochemical environments in the real structure of Na-bearing A–B carbonate apatites. The short O5–O8 distance (1.91 Å) remaining in the alternative defect cluster configuration (Fig. 5a) would be a destabilizing feature for the type A carbonate ion and, therefore, might also result in displacement of the type A v_3 bands to lower wavenumbers. However, this feature is also present in Na-free type A–B apatites like PC55 (Fig. 6).

4.4. Biomineralisation

The present synthetic apatite LM006 is similar in both composition and IR spectrum to bovine bone and human dental enamel (Table 7; Figs. 2 and 6) [5,9,14]. Therefore, the structure of this type A–B carbonate apatite is probably a good approximation to the structure of carbonated hydroxyapatite in bone and enamel. All these materials are Na-bearing carbonate apatites, and their IR spectra are characterized by v_3 absorption more-or-less confined to the 1400–1500 cm^{-1} spectral interval. The criteria established in the literature [5,23] for characterizing dominance by type B carbonate apatite (i.e. absence of significant v_3 absorption intensity beyond 1500 cm^{-1} and dominance of the 873 cm^{-1} band in the v_2 region) surely have to be revised in light of the present study which shows that the proportion of type A

carbonate in A–B apatites is sensitively dependent on the composition of the large cation positions, and particularly on the Na content. Also, the 873 cm^{-1} v_2 band is not proportional to the content of type B carbonate in all carbonate apatites, because it is dominant in all FTIR spectra of this study yet the X-ray structures show that type A carbonate is actually somewhat more abundant than type B in both LM005 and LM006 (Table 6). Type A carbonate is generally assumed to be only a minor component of dental enamel; e.g. 11% or 15%, based largely on the area of the weak ~1545 cm^{-1} IR band [5]. However, these low estimates for type A carbonate in bone and enamel have to be revised upward in light of the present study. Biological apatites are not type B carbonate apatites. Instead, they appear to be Na-bearing type A–B carbonate apatites; the mineral equivalent of LM006. Comparison with the v_3 region absorption for Na-bearing carbonate apatites (Fig. 6) shows that the type A carbonate component could account for up to 50% of total carbonate in biological apatites. Since channel constituents are more readily available for external reactions than carbonate substituting for the phosphate group, such high contents of type A carbonate could have profound consequences for the participation of biological apatites in biochemical processes.

5. Conclusions

The chemical compositions, single-crystal X-ray structures and FTIR spectra for a suite of Na-bearing type A–B carbonate apatites synthesized at 1200 °C and 0.5–1.0 GPa indicate coupling between Na cations and channel (type A) and phosphate (type B) carbonate ions at all carbonate contents investigated. The type B carbonate ion is located close to the sloping faces of the substituted phosphate tetrahedron, but inclined at an angle of 53° to the mirror plane. Coupling of A and B carbonate ion defects and tilting of the B carbonate ion in hydroxyapatite are required by the close approach (1.14 Å) of the off-axis oxygen of the channel carbonate ion to an O3 atom of the phosphate group.

The use of FTIR spectra to estimate the proportion of type A carbonate in synthetic apatites and biomineralisation is limited by dependence on the composition of the large cation (Ca1, Ca2) positions. The present Na-bearing type A–B apatites are characterized by asymmetric stretch (v_3) bands at 1400–1500 cm^{-1} and a dominant out-of-plane bend (v_2) band at 873 cm^{-1}. These synthetic apatites are chemical and structural models for biological apatites, which are reinterpreted as Na-bearing type A–B apatites with channel (type A) carbonate accounting for up to 50% of total carbonate.

Acknowledgments

We thank two anonymous referees for helpful comments, and the Natural Sciences and Engineering Research Council of Canada for financial support.

References

[1] Barralet J, Best S, Bonfield W. Carbonate substitution in precipitated hydroxyapatite: an investigation into the effects of reaction temperature and bicarbonate ion concentration. J Biomed Mater Res 1998; 41:79–86.
[2] Penel G, Leroy G, Rey C, Bres E. MicroRaman spectral study of the PO_4 and CO_3 vibrational modes in synthetic and biological apatites. Calcif Tissue Int 1998;63:475–81.
[3] Dowker SEP, Anderson P, Elliott JC, Gao XJ. Crystal chemistry and dissolution of calcium phosphate in dental enamel. Miner Mag 1999; 63:791–800.
[4] Dorozhkin SV, Epple M. Biological and medical significance of calcium phosphates. Angew Chem Int Ed 2002;41:3130–46.
[5] Elliott JC. Calcium phosphate biominerals. In: Kohn MJ, Rakovan J, Hughes JM, editors. Phosphates: reviews in mineralogy and geochemistry, vol. 48. Washington, DC: Mineralogical Society of America; 2002. p. 427–53.
[6] Gross KA, Berndt CC. Biomedical application of apatites. In: Kohn MJ, Rakovan J, Hughes JM, editors. Phosphates: reviews in mineralogy and geochemistry, vol. 48. Washington, DC: Mineralogical Society of America; 2002. p. 631–72.
[7] Suchanek WL, Shuk P, Byrappa K, Riman RE, TenHuisen KS, Janas VF. Mechanochemical–hydrothermal synthesis of carbonated apatite powders at room temperature. Biomaterials 2002;23:699–710.
[8] Wilson RM, Elliott JC, Dowker SEP, Smith RI. Rietveld structure refinement of precipitated carbonate apatite using neutron diffraction data. Biomaterials 2004;25:2205–13.
[9] Elliott JC. Structure and chemistry of the apatites and other calcium orthophosphates. Amsterdam: Elsevier; 1994.
[10] Bonel G. Contribution à l'étude de la carbonatation des apatites. I. Synthèse et étude des propriétés physico-chimiques des apatites carbonatées du type A. Ann Chim (Paris, France) 1972;7:65–88.
[11] Elliott JC. The interpretation of the infra-red absorption spectra of some carbonate-containing apatites. In: Fearnhead RW, Stack MV, editors. Tooth enamel: its composition, properties, and fundamental structure. Bristol, UK: Wright; 1964. p. 20–2.
[12] Elliott JC, Bollet-Quivogne FRG, Anderson P, Dowker SEP, Wilson RM, Davis GR. Acidic demineralization of apatites studied by scanning X-ray microradiography and microtomography. Miner Mag 2005;69:643–52.
[13] LeGeros RZ, Trautz OR, Klein E, LeGeros JP. Two types of carbonate substitution in the apatite structure. Experimentia 1969; 25:5–7.
[14] Jonas K, Vassanyi I, Ungvari I. The study of synthetic carbonate-hydroxyapatites and dental enamels by IR and derivative methods. Phys Chem Miner 1980;6:55–60.
[15] Nelson DGA, Featherstone JDB. Preparation, analysis, and characterization of carbonated apatites. Calcif Tissue Int 1982;34:S69–81.
[16] Nelson DGA, Williamson BE. Low-temperature laser Raman spectroscopy of synthetic carbonated apatites and dental enamel. Aust J Chem 1982;35:715–7.
[17] Vignoles M, Bonel G, Holcomb DW, Young RA. Influence of preparation conditions on the composition of type B carbonated hdroxyapatite and on the localization of the carbonate ions. Calcif Tissue Int 1988;43:33–40.
[18] Beshah K, Rey C, Glimcher MJ, Schimizu M, Griffin RG. Solid state carbon-13 and proton NMR studies of carbonate-containing calcium phosphates and enamel. J Solid State Chem 1990;84:71–81.
[19] Shimoda S, Aoba T, Moreno EC, Miake Y. Effect of solution composition on morphological and structural features of carbonated calcium apatites. J Dent Res 1990;69:1731–40.
[20] Regnier P, Lasaga AC, Berner RA, Han OH, Zilm KW. Mechanism of CO_3^{2-} substitution in carbonate-fluorapatite: evidence from FTIR spectroscopy, ^{13}C NMR, and quantum mechanical calculations. Am Miner 1994;79:809–18.

[21] Peeters A, De Maeyer EAP, Van Alsenoy C, Verbeeck RMH. Solids modeled by ab initio crystal-field methods. 12. Structure, orientation and position of A-type carbonate in a hydroxyapatite lattice. J Phys Chem B 1997;101:3995–8.
[22] Wilson RM, Elliott JC, Dowker SEP. Rietveld refinement of the crystallographic structure of human dental enamel apatites. Am Miner 1999;84:1406–14.
[23] Wilson RM, Dowker SEP, Elliott JC. Rietveld refinements and spectroscopic structural studies of a Na-free carbonate apatite made by hydrolysis of monetite. Biomaterials 2006;27:4682–92.
[24] Comodi P, Liu Y. CO_3 substitution in apatite: further insight from new crystal-chemical data of Kasekere (Uganda) apatite. Eur J Miner 2000;12:965–74.
[25] Suetsugu Y, Shimoya I, Tanaka J. Configuration of carbonate ions in apatite structure determined by polarized infrared spectroscopy. J Am Ceram Soc 1998;81:746–8.
[26] Suetsugu Y, Takahashi Y, Okamura FP, Tanaka J. Structure analysis of A-type carbonate apatite by a single-crystal X-ray diffraction method. J Solid State Chem 2000;155:292–7.
[27] Leventouri Th, Chakoumakos BC, Moghaddam HY, Perdikatsis V. Powder neutron diffraction studies of a carbonate fluorapatite. J Mater Res 2000;15:511–7.
[28] El Feki H, Savariault JM, Ben Salah A, Jemal M. Sodium and carbonate distribution in substituted calcium hydroxyapatite. Solid State Sci 2000;2:577–86.
[29] Ivanova TI, Frank-Kamenetskaya OV, Kol'tsov AB, Ugolkov VL. Crystal structure of calcium-deficient carbonated hydroxyapatite. Thermal decomposition. J Solid State Chem 2001;160:340–9.
[30] Fleet ME, Liu X. Carbonate apatite type A synthesized at high pressure: new space group ($P\bar{3}$) and orientation of channel carbonate ion. J Solid State Chem 2003;174:412–7.
[31] Fleet ME, Liu X. Location of type B carbonate ion in type A–B carbonate apatite synthesized at high pressure. J Solid State Chem 2004;177:3174–82.
[32] Fleet ME, Liu X, King PL. Accommodation of the carbonate ion in apatite: an FTIR and X-ray structure study of crystals synthesized at 2–4 GPa. Am Miner 2004;89:1422–32.
[33] Fleet ME, Liu X. Local structure of channel ions in carbonate apatite. Biomaterials 2005;26:7548–54.
[34] Peroos S, Du Z, de Leeuw NH. A computer modelling study of the uptake, structure and distribution of carbonate defects in hydroxyapatite. Biomaterials 2006;27:2150–61.
[35] Tyliszcak T. BAN Data analysis program. McMaster University, 1992.
[36] Morgan H, Wilson RM, Elliott JC, Dowker SEP, Anderson P. Preparation and characterization of monoclinic hydroxyapatite and its precipitated carbonate apatite intermediate. Biomaterials 2000;21:617–27.
[37] Elliott JC, Wilson RM, Dowker SEP. Apatite structures. In: Huang TC, editor. Advances in X-ray analysis, vol. 45. Newtown Square, PA: International Centre for Diffraction Data; 2002. p. 172–81.
[38] Santos M, Gonzalez-Diaz PF. A model for B carbonate apatite. Inorg Chem 1977;16:2131–4.
[39] White WB. The carbonate minerals. In: Farmer VC, editor. The infrared spectra of minerals. Monograph 4. London: Mineralogical Society; 1974. p. 227–84.